Modular mRNA lipid nanoparticle platform rescues diverse genetic male infertility

Qi Kai Jiang[1#], Kexin Su[2#], Huali Luo[3], Hao Wang[4], Jingwen Luo[1], Yukai Jason Zhong[1], Qiaodan Li[4], Zhihui Zhang[5], Haifeng Zhang[1], Banghua He[6], Linlin Zhang[6], Qin Li[1], Liang Xu Ma[1], Hongxiao Cui[1], Jiaoyan Ma[1], Xianguang Yang[6], Lejun Li[7], Zhefan Yuan[8], Shuai Liu[2], and Xin Zhiguo Li[1*]

[1]Center for RNA Medicine, International Medical School, International Institutes of Medicine, The Fourth Affiliated Hospital, Zhejiang University School of Medicine, Yiwu, Zhejiang, 322000, China.

[2]College of Pharmaceutical Sciences, State Key Laboratory of Advanced Drug Delivery and Release Systems, Zhejiang University, Hangzhou, 310058, China.

[3]Department of Pathology, The Fourth Affiliated Hospital, Zhejiang University School of Medicine, International Medical School, International Institutes of Medicine, Zhejiang University, Yiwu, Zhejiang, 322000, China.

[4]Center for Reproductive Medicine, The Fourth Affiliated Hospital, Zhejiang University School of Medicine, International Medical School, International Institutes of Medicine, Zhejiang University, Yiwu, Zhejiang, 322000, China.

[5]Department of Laboratory Medicine, The Fourth Affiliated Hospital, Zhejiang University School of Medicine, International Medical School, International Institutes of Medicine, Zhejiang University, Yiwu, Zhejiang, 322000, China.

[6]College of Life Sciences, Henan Normal University, Xinxiang, Henan, 453002, China.

[7]Department of Reproductive Endocrinology, Women's Hospital, Zhejiang University School of Medicine, Hangzhou, Zhejiang, 310006, China.

[8]CybernaX Biotechnologies, Hangzhou, Zhejiang, 311200, China.

[#]These authors contributed equally to this work.

*Correspondence: XinLiRNA@zju.edu.cn(X.Z.L.)

Abstract

Genetic male infertility affects millions worldwide and arises from diverse underlying mutations. Therapeutic mRNA holds promise, but remains challenged by a blood-testis barrier, immune privilege, dynamic post-transcriptional regulation, and multigenerational safety concerns. Here, we establish a modular mRNA-lipid nanoparticle (LNP) platform that rescues spermatogenesis across multiple genetic infertility models—including *Papolb*, *Spo11*, and *Btbd18* mutants—via protein replacement without genomic integration. Using FDA-approved MC3 LNPs, we achieved sustained mRNA expression (≈2 weeks) and germ cell-specific translation, outperforming newer vaccine lipids (SM-102 and ALC-0315). A single intratesticular injection of optimized, modified *Papolb* mRNA restored spermatid elongation in ~25% of tubules, and intracytoplasmic injection of rescued sperm produced healthy, fertile offspring across multiple generations. We further demonstrate that the same MC3-based LNP system enables efficient mRNA delivery into cultured human seminiferous tubules, supporting translational feasibility. Together, these findings demonstrate a clinically translatable mRNA therapeutic modality for genetic infertility and underscore a key nanotechnological principle: optimal extrahepatic LNP performance depends critically on the biological context.

.

Male infertility is a major public health problem with highly heterogeneous causes, affecting ~9% of reproductive-age men in the United States[1] and ~11% in China[2]. Nearly half of cases are idiopathic but thought to have a genetic basis, as spermatogenesis is regulated by more than 4,000 genes[3–5]. This complexity underscores the need for therapies that address specific genetic lesions rather than one-size-fits-all approaches. Assisted reproductive technologies (ART), such as in vitro fertilization (IVF) or intracytoplasmic sperm injection (ICSI), enable some men to father children but fail in more than half of treatment cycles[6] and remain inapplicable in the absence of viable sperm. About one third of couples never achieve a live birth despite repeated attempts[7]. For these patients, options are limited to donor gametes or childlessness, highlighting the urgent need for molecular therapies that restore endogenous spermatogenesis.

Messenger RNA (mRNA) therapeutics offer a programmable and transient means to restore protein expression without altering the genome. Spermatogenesis is highly dynamic—each human seminiferous cycle restarts every 72 days[8] and hundreds of seminiferous tubules generate tens of millions of sperm daily[9]—so the transient nature of mRNA aligns with the temporal demands of spermatogenic development. Even a brief restoration of a missing protein could generate enough functional sperm for assisted reproduction. Unlike DNA-based gene therapies, which raise ethical and safety concerns in germ cells[10], mRNA acts in the cytoplasm, and is not inherited. Unlike small molecule drugs, mRNA medicine can be flexibly reprogrammed for diverse genetic targets using the same delivery, design and manufacturing platform. Furthermore, the clinical window is flexible because there is no immediate life-threatening urgency; treatment outcomes are easily monitored via semen analysis, and recovered sperm can be cryopreserved.

However, applying mRNA therapy to germ cells poses unique challenges. The testes are immune-privileged and protected by the blood–testis barrier (BTB), which restricts drug penetration and shields developing germ cells[11,12]. Moreover, meiotic and post-meiotic germ cells store large pools of untranslated mRNAs under tight temporal control[13].

Exogenous mRNAs may therefore fail to be translated or may be rapidly degraded. Safety is another paramount concern, as sperm RNAs carry epigenetic information that influences offspring development[14,15], and rare events of reverse transcription and genomic integration have been described[16]. Together, these hurdles have kept testicular mRNA therapy largely unexplored.

A previous mouse study delivering a self-amplifying mRNA via novel lipid nanoparticles (LNPs) restored spermatogenesis but failed to restore fertility[17]. A very recent study has demonstrated a critical advance: a custom LNP-mediated delivery of *Pdha2* mRNA, engineered for germ cell-biased expression using microRNA target sequences, successfully restored meiosis, produced sperm, and yielded healthy, fertile F1 offspring via ICSI in a mouse model of non-obstructive azoospermia[18]. While this breakthrough confirms the therapeutic potential of the approach, it also delineates the next frontier of challenges: the systematic optimization of both LNP composition and the RNA design for durable expression, comprehensive evaluation of long-term and transgenerational safety, development of a generalizable platform effective across distinct genetic etiologies, and—most critically—demonstration of efficient and safe delivery in human tissues, which is essential for clinical translation.

Here, we build on these foundational advances and close several of these critical gaps. We first performed a head-to-head comparison of clinically approved LNP formulations for intratesticular delivery. Contrary to the prevailing assumption that newer lipids such as ALC-0315 and SM-102 are universally superior, we found that the FDA-approved DLin-MC3-DMA (MC3) — the same lipid used in the siRNA therapeutic *patisiran* — uniquely enabled efficient, testis-restricted delivery with minimal immunogenicity. Having identified MC3 as the optimal carrier, we then systematically compared RNA modalities—unmodified mRNA, N1-methylpseudouridine-modified mRNA, self-amplifying RNA, and circular RNA—establishing that modified mRNA provides the optimal combination of high-level protein expression and low

immunogenicity. Through careful optimization of dose and regimen, we found that a single injection of this optimized MC3-modified mRNA platform fully restored spermiogenesis in *Papolb*-deficient mice, producing functional sperm without genomic editing. The resulting offspring were healthy and fertile through multiple generations. We further demonstrated the platform's modularity by partially rescuing spermatogenesis in two additional infertility models (*Spo11* and *Btbd18* mutants). Importantly, as a critical step toward clinical translation, we established efficient mRNA delivery in temporally cultured human testicular tissues. Together, these findings provide the first demonstration of a modular, clinically relevant mRNA–LNP platform capable of correcting diverse genetic causes of male infertility, while revealing a general nanotechnological principle: lipid performance is context-dependent, and indication-specific carrier and RNA-platform selection is essential for enabling extrahepatic mRNA therapeutics.

Results

Localized mRNA delivery to the testis

Delivering genetic material into the immune-privileged testis is challenging owing to the blood-testis barrier (BTB) and specialized seminiferous tubule architecture. We first compared four non-viral approaches—direct electroporation, protamine-mediated transfection, red blood cell membrane (RBCM) vesicle encapsulation, and lipid nanoparticles (LNPs)—for delivering mRNA to adult mouse testes. Despite protamine's ability to form cationic nanocomplexes with mRNA[19] and previous use of intratesticular electroporation to introduce DNA[20,21], none of the combinations tested (naked mRNA, protamine-condensed mRNA, electroporation, RBCM vesicle encapsulation, or combinations thereof) yielded more than background-level luminescence in the testis. Only the fully combined method (mRNA + RBCM + electroporation) produced a detectable but weak luciferase signal, suggesting poor tissue penetration and inefficient release of mRNA (Supplementary Fig. 1a, b).

In contrast, LNPs—vehicles that have revolutionized nucleic acid delivery in recent vaccines and therapeutics—showed markedly superior delivery efficacy in the testis (Fig. 1a). To maximize delivery across the BTB and limit systemic exposure, we compared interstitial versus intratubular routes of injection. Infusion into the efferent duct (rete testis) uniformly filled seminiferous tubules and yielded 2.3–6.1-fold higher luciferase activity than interstitial injection at equivalent doses at 6–24 h post-injection ($p < 0.01$; Fig. 1a). Efferent duct infusion was well tolerated, causing only transient swelling, and exposed germ cells directly to nanoparticles without the large doses needed for systemic administration. We therefore adopted intratubular administration for subsequent experiments.

Selection and characterization of optimized LNP formulations

LNPs employ ionizable lipids to condense RNA and promote endosomal escape. We formulated three clinically validated ionizable lipids—DLin MC3 DMA (MC3), ALC-0315 and SM-102—with helper lipids (DSPC, cholesterol, PEG-lipid). All yielded ~100–106 nm particles with low polydispersity and near-neutral ζ-potentials (–3 to –6 mV; Supplementary Fig. 1c). Encapsulation efficiencies for luciferase mRNA were 94–98 % (Supplementary Fig. 1c). Transmission electron microscopy (TEM) further confirmed that all LNPs exhibited broadly similar morphology, with no gross structural differences across lipid types (Supplementary Fig. 1d). These comparable physicochemical and morphological parameters enabled a fair and rigorous head-to-head in vivo comparison of lipid performance.

Following intratubular injection, SM-102 and ALC-0315 LNPs mediated higher testis-localized luciferase signals than MC3, with SM-102 peaking by 6 h and MC3 and ALC-0315 peaking later (Fig. 1b,c). However, SM-102 produced a prominent off-target signal in the liver and spleen despite local delivery (Fig. 1b,c). This “liver leak” persisted even at a 75 % lower dose (Supplementary Fig. 1e), indicating an intrinsic distribution difference for that formulation, echoing reports that SM-102 can access hepatic

compartments when given intramuscularly in vaccines[22]. Notably, MC3 is optimized for hepatic delivery of siRNAs (e.g. the drug Onpattro)[23]; thus this off-target liver transfection specific to SM-102 was unexpected after local injection. The SM-102 formulation either penetrates the BTB more readily or is less retained within the seminiferous tubules, allowing a significant portion of the dose to escape into the bloodstream.

We quantified innate immune activation after LNP injection. At 12 h post-delivery, SM-102 LNP induced substantial upregulation of *Tnf-α*, *Cxcl10*, *IL-6*, *Ifnb1*and *IL-1β*, comparable to the lipopolysaccharide (LPS) positive control (Fig. 1d), and gross examination revealed testicular erythema and swelling (Fig. 1e, f). MC3 and ALC-0315 LNPs elicited only mild cytokine induction and minimal histological inflammation (Fig. 1d, f). No obvious differences were observed in other organs (Supplementary Fig. 1f). Thus, MC3 and ALC-0315 provided efficient and well-tolerated testis delivery, whereas SM-102 triggered off-target hepatic transfection and inflammation. These observations underscore that LNP composition and tissue context, rather than lipid "generation", determine biodistribution and immunogenicity.

Germ cell–specific targeting across spermatogenesis

We next determined which testicular cell types were transfected. In Ai9 reporter mice (Rosa26 LoxP-STOP-LoxP tdTomato), Cre mRNA delivered via MC3 or ALC-0315 LNP induced robust tdTomato expression exclusively in the injected testis, whereas SM-102 again generated off-target liver and spleen signals with concomitant testicular inflammation (Fig. 2a; Supplementary Fig. 2a–c). High-magnification imaging showed tdTomato in spermatogonia, spermatocytes and spermatids, as well as in Sertoli cells identified by SOX9 staining (Fig. 2b). Flow cytometry further confirmed that >90 % of cells in each germ cell subpopulation (haploid, diploid and tetraploid) were tdTomato^{+} after MC3 or ALC-0315 LNP delivery (Fig. 2c; Supplementary Fig. 2d, e). Thus, optimized LNPs efficiently transfect germ cells throughout spermatogenesis.

Modified mRNA for sustained expression and low immunogenicity

We compared three MC3 LNP–delivered RNA formats encoding eGFP. These included a chemically modified mRNA (incorporating N^1 methylpseudouridine with a cap 1 structure and poly(A) tail), a self-amplifying mRNA (saRNA) replicon, and a circular RNA (circRNA). The modified mRNA produced the highest peak GFP expression within three days, whereas the saRNA and circRNA yielded lower peak levels. Notably, the latter two formats elicited elevated innate immune responses at 24 hours but sustained only low-level expression through day 14 (Fig. 2d; Supplementary Fig. 2f, g). Because sperm RNAs are known to mediate epigenetic information to offspring[14,15], we sought to avoid the potential for heritable effects from unnecessary prolonged RNA expression in the germline. We therefore chose to use linear mRNA, which provides transient yet robust expression, rather than RNA formats that drive extended expression.

Because nucleoside modifications can increase frameshift or read-through translation events[24] and the testis is an immune-privileged organ[25,26], we next compared unmodified mRNA to pseudouridine-modified mRNA. The unmodified mRNA produced a rapid burst of eGFP expression that declined by day 3, whereas the modified mRNA peaked at day 3 and remained detectable through day 7 (Fig. 2e; Supplementary Fig. 2k). RT-qPCR analysis further confirmed the greater stability of the modified mRNA (Fig. 2f). However, even in the immune-privileged testis—characterized by low TLR7/8 expression and local immunosuppression[25,26]—the unmodified mRNA provoked a potent innate immune activation. This was evidenced by >10-fold induction of *Tnf-α*, *Cxcl10*, *IL-6*, *Ifnb1*, and *IL-1β*, whereas the modified mRNA elicited only minimal cytokine responses (Fig. 2g). In light of these results, we elected to use N^1 methylpseudouridine–modified mRNA for all subsequent therapeutic experiments to maximize protein expression and minimize innate immune activation.

Delivery of optimized endogenous mRNA achieves correct localization and undetectable toxicity

We selected *Papolb* (also known as *Tpap*) as a model genetic infertility target because it encodes the testis-specific cytoplasmic poly(A) polymerase PAPOLB. Male *Papolb* mutants exhibit spermatogenic arrest at the round spermatid stage and are infertile[27]. We designed an optimized Papolb mRNA incorporating codon optimization while retaining the endogenous 5´UTR and adding a heterologous stabilizing human α-globin 3´UTR (Fig. 3a). We also included a small HA epitope tag to facilitate detection, which did not affect PAPOLB's in vivo function[28].

After confirming mRNA quality (integrity, ≤0.005% dsRNA; endotoxin < 4 EU mL^{-1}; Supplementary Fig. 3a, b), we formulated the mRNA into MC3 and ALC 0315 lipid nanoparticles (LNPs). In wild-type mice, both MC3 and ALC 0315 LNPs successfully delivered HA–PAPOLB expression to the germ cell cytosol within 10 h, with the protein produced at the expected molecular weight (Fig. 3b, c). Importantly, this germline expression did not disrupt testis or epididymis morphology (Supplementary Fig. 3c). Furthermore, HA–PAPOLB was undetectable in other organs (Supplementary Fig. 3d), indicating that translation was restricted to germ cells. Our data confirm that the engineered *Papolb* mRNA is specifically expressed in germ cells without perturbing spermatogenesis.

LNP–mRNA therapy rescues spermiogenesis in a male infertility model

We administered a single intratubular injection of *Papolb* mRNA–LNP (without the HA tag) to *Papolb* knockout males. By day 7, MC3 LNP restored spermatid differentiation, evidenced by elongating spermatids in many seminiferous tubules (Fig. 4a). The transition from round to elongated spermatids was confirmed by protamine-1 and acrosome (PNA) staining (Fig. 4b). In contrast, ALC 0315 LNP failed to rescue spermiogenesis at any time point (Fig. 4b; Supplementary Fig. 4a).

To investigate the functional differences between the two LNPs, we compared their performance in detail. We found that MC3-delivered mRNA persisted much longer than ALC 0315-delivered mRNA, with HA–PAPOLB protein detectable for ~10 days versus ~3 days by immunofluorescence (Fig. 3b) and ~4 days versus ~2 days by western blot (Fig. 3c). RT-qPCR revealed that MC3 LNP-delivered *Papolb* mRNA persisted for ~14 days post injection, whereas ALC 0315 LNP-delivered mRNA dropped below detectable levels by ~5 days (Fig. 3d). Although detection limits differ between assays, all methods point to the same conclusion: MC3 LNP provides a longer duration of expression than ALC 0315. Given the prolonged expression of MC3-delivered mRNA compared to ALC 0315-delivered mRNA (Fig. 3b–d), these data suggest that the duration of expression, rather than peak delivery efficiency, governs therapeutic efficacy in this *Papolb* knockout model.

Dose–response studies revealed that 0.4 mg mL^{-1} (~8 µg per testis) MC3– *Papolb* mRNA maximally rescued ~25 % of tubules (Fig. 4c,d). This rescue was validated by protamine-1 and PNA staining (Supplementary Fig. 4b), and improvement was further quantified by epithelial height, Johnsen scores and testis weight as well as decreased apoptosis (Fig. 4d, Supplementary Fig. 4c). Higher doses caused toxicity with elevated inflammation, significantly increased apoptosis without improving rescue (Supplementary Fig. 4c, d Fig. 4c, d). Temporal analysis showed that elongating spermatids appeared by day 7, peaked at days 9–13 and declined by day 15; by day 17 tubules reverted to the arrest phenotype (Fig. 4e). Epithelial height, Johnsen scores and testis weight as well as protamine-1 and PNA staining mirrored this transient wave (Supplementary Fig. 4e, f). The transient effect matches the seminiferous epithelial cycle (~207 h, Supplementary Fig. 4g)[29], indicating that mRNA-rescued tubules undergo normal spermatogenesis. Multiple dosing, while extending the duration of sperm production, did not increase the percentage of rescued tubules (Supplementary Fig. 4h), suggesting a single injection is already sufficient to “jump-start” one cohort of spermatids.

Restoration of fertility and generation of healthy offspring

Rescued males produced testicular sperm with normal head–tail morphology and motility, indistinguishable from testicular sperm isolated from heterozygous *Papolb*$^{+/-}$ males (fertile littermate controls) (Fig. 5a and Supplementary Video). Because efferent duct surgery likely prevented sperm transit to the epididymis (Supplementary Fig. 5a–c), we used ICSI to assess fertility. Testicular sperm from MC3-treated *Papolb*$^{-/-}$ males successfully fertilized wild-type oocytes, yielding ~79 % two-cell embryos—comparable to testicular sperm from heterozygous controls (~83 %) and slightly lower than epididymal sperm (~97 %; Fig. 5b, c). Embryo transfer produced live F1 offspring (nicknamed "Papi" from inherited *Papolb* deficiency) at a ~20 % success rate, similar to controls (Fig. 5c). Papi pups exhibited normal postnatal growth (Fig. 5d, Supplementary Fig. 5e). All offspring from treated sires were heterozygous carriers, consistent with an unedited germline (Supplementary Fig. 5d), and showed no evidence of genomic integration from reverse-transcribed *Papolb* mRNA (Fig. 5e).

We next systematically assessed long-term safety. Gross and histological examination of 19 organs showed no abnormalities in Papi mice (Supplementary Fig. 5f). Body composition analyses (weight, lean/fat percentage, bone mass, bone density) revealed no differences (Supplementary Fig. 5g). Haematology and serum chemistry metrics were comparable (Supplementary Fig. 5h, i). Behavioral tests (open field, object recognition, novel object exploration) showed no differences in anxiety-like behaviour or memory between Papi and controls (Fig. 5f; Supplementary Fig. 5j). Sexual behaviour (mounting latency, intromission latency, copulatory duration) was similar between Papi and heterozygous controls (Supplementary Table 1). Importantly, Papi proved fertile and sired healthy F2 offspring with normal pup size and growth (Fig. 5g, h; Supplementary Fig. 5k). We further measured testosterone and FSH levels in both Papi and F2 progeny, all of which fell within the normal range (Supplementary Fig. 5l), and successfully produced viable F3 offspring (Fig.5i) — confirming that the F2 generation was fertile.

Collectively, these data demonstrate multigenerational safety and functional fertility rescue without detectable adverse effects.

Generalizability to other genetic defects and human tissue

To assess broader applicability, we applied our engineered mRNA–LNP strategy (Fig. 3a) — incorporating codon optimization, retention of the endogenous 5´UTR, and a heterologous stabilizing human α-globin 3´UTR — using our optimized MC3 LNP formulation in two additional male-infertility models. The first, *Spo11*, which encodes a key enzyme for double-strand break formation during meiosis, causes meiotic arrest when mutated[30,31]. The second, *Btbd18* is required for piRNA precursor transcription; its loss arrests spermatogenesis at the round spermatid stage[32]. In *Spo11* mutants (meiotic defect), MC3 LNP–mRNA delivery induced round spermatids by day 15 and elongated spermatids by day 21 (Fig. 6a). In *Btbd18* knockouts (piRNA pathway defect), treatment induced elongating spermatids by day 13 to 19 (Fig. 6b). The longer time required to achieve elongation is expected, given that *Spo11* mutants arrest at an earlier stage of spermatogenesis compared with the *Papolb* and *Btbd18* mutants. Additional immunostaining with PNA (acrosome marker) and protamine1 (post-meiotic marker) further confirmed restoration of late-stage spermiogenesis in both models (Fig. 6c, d), also without sperm in epididymis (Supplementary Fig. 6a, b). Although further optimization of mRNA design, dosage, and timing will likely be needed for each gene, these results demonstrate that our platform extends beyond a single mutation and offers potential for individualized, precision treatment of diverse spermatogenic defects.

To translate toward human application, we established short-term culture of human seminiferous tubules obtained from fertility-clinic specimens. Incubation with MC3-LNPs carrying luciferase mRNA produced no dramatic morphological change or elevated cell death (Supplementary Fig. 6c). After addition of LNPs directly to the culture medium, immunostaining revealed luciferase expression within human germ cells at 24 h, with reduced but still detectable expression at 48 h (Fig. 6e, f), the timing paralleling our

mouse observations (Fig. 1b) and supporting the translational potential of our platform in human tissue.

Discussion

Our study establishes a modular mRNA-LNP platform that rescues spermatogenesis and fertility across diverse genetic models of male infertility, without genomic alteration. Building upon the recent demonstration that LNP-mediated mRNA delivery can address infertility in a single-gene model[18], our work provides the foundational nanotechnological optimization and generalization of this approach. By systematically comparing clinically relevant LNP formulations, we identified the FDA-approved MC3 lipid as uniquely capable of overcoming the testis's biological barriers—including the blood-testis barrier, post-meiotic translational repression, and innate immune surveillance—to achieve sustained mRNA expression. A single injection of our optimized, N^1-methylpseudouridine–modified *Papolb* mRNA restored spermatid maturation, enabling the production of functional sperm for ICSI and yielding healthy, fertile offspring through multiple generations. This rescue was not isolated to a single defect; we further demonstrated the platform's modularity in two additional infertility models (*Spo11*, *Btbd18*), and confirmed its potential for clinical translation by achieving efficient mRNA delivery in cultured human testicular tissues. Crucially, the therapy was transient and non-integrating, preserving genomic integrity and affirming the safety of this nanotherapeutic strategy across generations.

From a nanotechnology perspective, our work reveals a critical design principle: LNP efficacy is an intrinsic property of the lipid, but an emergent function of its release kinetics, tissue retention, and immunogenicity align with the target tissue. While next-generation lipids like SM-102 and ALC-0315—celebrated for their branched-tail, ester-linked designs that promote biodegradability and potent endosomal escape—often outperform the first-generation MC3 lipid in standard hepatic and muscular delivery models[33–39], we observed a striking inversion of this hierarchy in the testis. In our head-

to-head comparison, only MC3-LNPs achieved functional fertility rescue. SM-102 and ALC-0315 formulations, despite robust initial expression, provoked local inflammation and leaked mRNA systemically, undermining therapeutic efficacy. We attribute MC3's unique success to its slower release kinetics and prolonged tissue retention, which create a sustained ~14-day expression window perfectly matched to the timescale of spermatid maturation. The near-two-week sustained extrahepatic mRNA expression is unprecedented for MC3, a lipid long considered liver-specific for siRNA therapeutics[40]. What further distinguishes our work is the systematic, side-by-side evaluation of MC3, SM-102, and ALC-0315 in a demanding non-hepatic context, measuring functional biological rescue rather than transient reporter output. Our demonstration that MC3 can support prolonged mRNA-driven protein functional rescue in an extrahepatic tissue underscores a fundamental advance: optimal lipid selection requires indication-specific screening, as "newer" does not universally equate to "better". This insight mandates a broader consideration, both new and legacy lipid formulation, for next-generation extrahepatic mRNA therapeutics.

The ability to transiently replace missing germ-cell proteins offers a new therapeutic paradigm for male infertility. The global male infertility treatment market, a multi-billion dollar industry, currently lacks curative solutions for genetic forms of the condition. Our results suggest that men with genetic forms of non-obstructive azoospermia could potentially father their own children through a minimally invasive testicular injection, reducing reliance on donor sperm. The clinical feasibility of this approach is supported by our demonstration of efficient mRNA delivery using the optimized MC3-LNP system in temporally cultured human testicular tissues. Because all components of our LNP are used in approved products and regulatory frameworks for mRNA therapies are well established, translation to the clinic appears highly promising. Off-the-shelf mRNAs could be prepared for common mutations, while bespoke mRNAs could be rapidly synthesized for rarer defects. The scrotal location of human testes should further facilitate

local administration with minimal systemic exposure, making the approach feasible even in resource-limited settings.

Several considerations and future directions emerge from our study. First, although rescued males produced functional sperm, they required ICSI with testicular sperm rather than natural conception, similar to the outcome in Mashiko et al.[18]. We believe this limitation arises because the microinjection procedure temporarily disrupts epididymal sperm transport or luminal continuity. In humans, with testis in the scrotum, ultrasound-guided injections could preserve sperm transport, potentially enabling natural conception or less invasive approaches such as intrauterine insemination[41]. Second, only ~25% of tubules showed rescue despite >90% cells with mRNA uptake. Our investigation into this ceiling effect revealed that multiple injections extended the duration of sperm production but did not increase the percentage of rescued tubules. This plateau suggests the limit is not a delivery failure but likely governed by the intrinsic synchronicity of the seminiferous cycle, where only a subset of tubules contain responsive spermatids at any given time. This biological constraint may generalize to other therapies in cyclic or renewing tissues (e.g. hair follicles, intestinal crypts), where only a fraction of replication units can respond at any given time. Third, both Mashiko et al.[18] and our work validate mRNA supplementation as a therapy for recessive loss-of-function defects. Because our LNP–mRNA platform is modular, one can in principle deliver siRNAs, suppressor tRNAs, multiple mRNAs, or mRNA–miRNA cassettes, enabling correction of dominant-negative mutations, multi-gene syndromes, or complex defects (e.g. Y-chromosome microdeletions). Finally, our approach shares a common limitation with other mRNA-based strategies: it requires the presence of germ cells. In patients with complete germ cell loss (Sertoli-cell–only syndrome), exogenous mRNA will be ineffective. For such cases, a combined approach may be necessary, for instance integrating mRNA therapeutics with in vitro gametogenesis or stem-cell–derived germ cell derivation[42]. Early diagnosis will also be crucial, so interventions occur before germ cells are entirely depleted. In sum, RNA therapeutics provide a flexible, non-integrating platform that —

when germ cells remain — can be adapted to a wide spectrum of genetic male infertility etiologies.

Beyond therapy, our testis-targeted delivery approach provides a powerful research tool for reproductive biology. Germ cells have historically been refractory to transfection, limiting functional studies. The ability to introduce nucleic acids directly into the adult testis now enables rapid gene perturbation in vivo. For example, Cre mRNA or CRISPR components could be delivered to dissect gene function during spermatogenesis, offering a virus-free complement to sgRNA library screens already demonstrated in mouse testes[43]. Similarly, mRNA reporters could probe post-transcriptional control in spermatids, or SNPs associated with infertility could be tested in situ. Making the testis genetically accessible will accelerate discovery and refine therapeutic strategies.

Importantly, our therapy is non-heritable and avoids the ethical dilemmas of germline editing. It restores a natural process within the treated individual without altering DNA transmitted to offspring. Children conceived through this approach inherit parental genes as usual, typically as healthy carriers of any recessive allele. Concerns about propagating "bad genes" are overstated, as most infertility mutations are rare, recessive, or de novo, and their population frequency is unlikely to increase. Indeed, some infertility-associated alleles may even provide heterozygote advantages (e.g., ΔF508 in cystic fibrosis conferring infection resistance[44]). Ensuring equitable access will be essential, as early gene therapies are often costly and infertility treatments are not universally covered by insurance. With demonstrated safety and efficacy, we anticipate this approach will be viewed as a necessary component of reproductive healthcare, offering men with genetic infertility the opportunity to have biological families.

In summary, our work establishes a modular and optimized mRNA-LNP platform that significantly advances the therapeutic potential demonstrated in recent studies. While foundational reports confirmed the viability of mRNA supplementation for male infertility, our study provides the critical nanotechnological optimization, demonstrating

that the FDA-approved MC3 lipid outperforms newer vaccine lipids in this extrahepatic context. This context-dependent LNP efficacy highlights the need for indication-specific carrier selection in developing extrahepatic mRNA therapeutics. Validated by efficient delivery in human testicular cultures and multi-generational safety, our platform enables functional gamete production across diverse genetic defects without genome editing. By providing both a versatile therapeutic strategy for untreatable infertility and a powerful research tool for reproductive biology, this work illustrates how mRNA therapeutics can harness natural regenerative processes, offering a new paradigm for regenerative medicine.

Methods

Nanoparticle formulation and characterization

Formulation:

Lipid nanoparticle (LNP) formulations were prepared by a rapid ethanol dilution method, similar to published protocols[45]. Briefly, an ionizable lipid (such as ALC-0315, SM-102, or MC3; obtained from UTgene, Cat# UT1001, UT1002, UT1003, respectively) and helper lipids – cholesterol (Sigma–Aldrich, C8667), 1,2-distearoyl-sn-glycero-3-phosphocholine (DSPC; Avanti, 850365P), ALC-0159 (AVT (Shanghai) Pharmaceutical Tech, Cat# 002009), and a polyethylene glycol conjugated lipid (PEG-lipid; AVT, Cat# 002005) – were dissolved together in absolute ethanol at defined molar ratios. MC3 LNPs were formulated with DLin-MC3-DMA, DSPC, cholesterol and DMG-PEG2000 at a molar ratio of 50:10:38.5:1.5. For SM-102 LNPs, the molar ratio of SM-102/DSPC/cholesterol/DMG-PEG2000 was 50:10:38.5:1.5. ALC-0315 LNPs were formulated with ALC-0315/DSPC/cholesterol/ALC-0159 at a molar ratio of 46.3:9.4:42.7:1.6. The nucleic acid cargo (e.g., mRNA) was diluted in an acidic buffer (10 mM citrate, pH ~4.0). The ethanol lipid solution was rapidly mixed with the aqueous RNA solution at a fixed 1:3 volume ratio (organic : aqueous) to promote spontaneous self-assembly of nanoparticles. The mixture was incubated at room temperature for ~10

minutes to allow vesicle formation. For in vivo use, the crude LNP suspension was further purified by dialysis against PBS to remove residual ethanol and any unencapsulated RNA, then concentrated in PBS by ultrafiltration to the desired nucleic acid concentration. The specific ionizable lipid and type of nucleic acid cargo used in each experiment are detailed in the Results (and figure legends). In general, the nucleic acid cargos included various mRNA constructs, a self-amplifying mRNA (saRNA), or a circular RNA (circRNA). The sources of these constructs were as follows: *Papolb* mRNA and saRNA were synthesized in-house by in vitro transcription; Cre mRNA was purchased from RNAlfa Biotech (Cat# Alfa-2501); firefly luciferase mRNA was from Levostar (Cat# LS-RM021); and the circRNA was obtained from Novoprotein (Cat# MR201-U100).

Characterization:

The hydrodynamic diameter and polydispersity index (PDI) of LNPs were measured by dynamic light scattering (DLS) using a Malvern Zetasizer Nano instrument. Samples were diluted in PBS and equilibrated at room temperature before analysis. Size is reported as the intensity-weighted mean diameter, with PDI as a measure of dispersity.

The surface æ-potential of the nanoparticles was determined on the same instrument using folded capillary cells, after diluting samples ~50-fold in deionized water.

Encapsulation efficiency of mRNA was assessed with a RiboGreen RNA fluorescence assay (Thermo Fisher Quant-iT™ RiboGreen kit), by treating aliquots of the LNP with or without 0.2% Triton X-100 to distinguish encapsulated vs. total RNA. Encapsulation efficiency (%) was calculated as 100 × (protected RNA / total RNA input).

Animal experiments

All animal procedures were performed in accordance with institutional and national guidelines for animal welfare and were approved by the Laboratory Animal Welfare and

Ethics Review Committee of Zhejiang University (ZJU20220156 and ZJU20250897). The protocol adhered to principles of humane care, and measures were taken to ensure animal well-being throughout the experiments. Housing conditions: temperature 20–26 °C, humidity 40–70%, 12 h light/dark cycle (lights on at 7:30; off at 19:30), normal chow diet, corn cob bedding, cage density of 5 mice per cage.

Mouse strains: Wild-type C57BL/6J mice (Jackson Laboratory, stock #000664) were used for most in vivo experiments. B6.Cg-*Gt(ROSA)26Sor*$^{tm9(CAG\text{-}tdTomato)Hze}$/J reporter mice (the Ai9 line; JAX stock #007909), *Papolb* knockout mice (*Papolb*$^{-/-}$) were obtained from RIKEN BioResource Center[27,46], *Spo11* knockout mice were constructed according to the previous publication[30], and *Btbd18* knockout strain[32] were maintained on a C57BL/6 background. Mice were genotyped by PCR on tail DNA (using primers provided by the source repository). To test the potential integration of *Papolb* mRNA, we used primers targeting the coding sequence of the delivered mRNA (which was codon-optimized, distinct from the genomic copy; primer sequences used for all genotyping were provided in Supplementary Table 2). Unless otherwise noted, experimental cohorts consisted of young adult male mice (aged over 6 weeks, average 25 g body weight) to ensure sexual maturity. Mice were randomly assigned to treatment groups, and investigators were blinded to group allocations during outcome assessments wherever possible (see Statistical analysis below). Number of animals per group: n = 3 for LNP delivery, rescue, and fertility; n = 5 for behavioral assays and sexual activity.

In vivo administration of nanoparticles / mRNA

Two delivery routes were used, depending on the target cell population: (1) injection via the rete testis/efferent duct to deliver material into the seminiferous tubules (targeting primarily Sertoli cells and germ cells), and (2) direct interstitial injection into the testis parenchyma (targeting Leydig cells and other interstitial cells). In each case, adult male mice were anesthetized with 2.5% tribromoethanol in PBS (Avertin, i.p., MeilunBio, MA0478) and placed supine on a sterile surgical platform. For the rete testis (tubular)

delivery, a small lower abdominal incision (~1 cm) was made to exteriorize the testis within the tunica. Using a dissecting microscope, the efferent ducts emerging from the testis (near the junction with the epididymis) were identified. A fine pulled-glass micropipette (tip diameter ~50–80 µm) pre-loaded with the RNA solution (with a trace of 0.05% Fast Green dye added for visibility) was carefully inserted into the lumen of the efferent duct. Approximately 20 µL of solution was slowly injected at 3–5 µL/sec; successful delivery into the seminiferous tubules was confirmed by observing the dye spreading from the rete testis throughout the tubules (visible as faint green coloration filling the testis) (Fig.1a). For interstitial injections, a 30-gauge needle (Hamilton syringe) was inserted directly into the testis parenchyma, and ~20 µL of solution was delivered into the interstitial space between tubules at the same rate. Care was taken to inject slowly and avoid excessive pressure to prevent tissue rupture or back-leakage. After either type of injection, the abdominal incision was closed with absorbable sutures. Analgesia: Ibuprofen (50–60 mg/kg/day; 10 mL of Children's Motrin in 500 mL of water) continuously in drinking water for 3 days post-surgery. Mice were monitored during recovery from anesthesia and returned to their home cages once fully ambulatory.

Dosing regimens

Doses of the nucleic acid cargo were selected based on preliminary studies and prior literature. Ai9 reporter mice received LNP-encapsulated Cre mRNA via tail vein injection at a dose of 10 µg mRNA per mouse (approximately 0.4 mg/kg body weight). For luciferase reporter studies, mice were administered firefly luciferase mRNA–LNP at 10 µg (0.4 mg/kg) (by intramuscular or intratesticular injection) as detailed in the Results section. *Papolb* knockout mice assigned to gene therapy received an i.t. dose of LNPs carrying *Papolb* mRNA at 0.32 mg/kg. In some experiments, self-amplifying mRNA (saRNA) or circular RNA (circRNA) formulations were administered via the same routes; the dosing for saRNA and circRNA (10 µg per testis, 0.4 mg/kg) was comparable to the mRNA doses. Control animals received equivalent volumes of vehicle (PBS). All

treatments were given as a single dose unless otherwise noted. No animals were excluded from analysis a priori except in the case of a technical failure (e.g., if an injection was visibly mis-delivered); in this study, no such exclusions were necessary. Body weights at dosing: 25 g. Dose-response experiments: *Papolb* KO mice received 2, 4, 8, or 16 µg *Papolb* mRNA–LNPs (n = 2 mice per dose). Samples were collected on day 7 post-injection. Time-course experiments: *Papolb* KO mice treated with 8 µg *Papolb* mRNA–MC3 LNPs were sampled at 7, 9, 11, 13, 15, 17, 19, and 21 days post-injection. *Btbd18* KO mice were sampled on day 13 and 19, and *Spo11* KO mice on day 15 and 21.

In vivo fluorescence and bioluminescence imaging

Fluorescence imaging (tdTomato reporter):

To evaluate nanoparticle biodistribution and transgene expression in vivo, mice were imaged using an IVIS Spectrum optical imaging system (BIOSPACE LAB Photon IMAGER Optima) at various time points after treatment. For the *Cre* mRNA delivery studies using Ai9 reporter mice, animals were euthanized, dissected and major organs (including testes, liver, spleen, kidneys, lungs, and heart) harvested for ex vivo fluorescence imaging at 48 hours post-injection. tdTomato fluorescence was captured using the appropriate excitation/emission filter settings (Ex 570 nm / Em 620 nm). Identical imaging parameters (illumination intensity, exposure time, binning, etc.) were used for all animals to allow quantitative comparison. Fluorescence intensity was quantified as radiant efficiency within regions of interest (ROIs) using M3Vision® software (BIOSPACE LAB).

Bioluminescence imaging (luciferase reporter):

For luciferase experiments, bioluminescence imaging was performed at designated timepoints. To compare different intratesticular injection routes (rete testis vs interstitial), images were collected at 6, 9, 12, and 24 h. To compare different LNP formulations (MC3, ALC-0315, SM-102) and assess SM-102 leakage, images were collected at 1, 3, 6, 9, 12, and 24 h post-injection. Mice were injected intraperitoneally with D-luciferin (150

mg/kg, 100 µL; Gold Biotechnology, LUCNA-100) and anesthetized with isoflurane 5 min later. Photons emitted from firefly luciferase activity were collected with a 5 s exposure, standard binning, and consistent field of view. Data were analyzed as total photon flux (photons/sec) within ROIs encompassing the testes or other relevant regions. Baseline auto-luminescence was negligible.

Tissue preparation and immunofluorescence microscopy

Frozen-section imaging of native tdTomato:
For high-resolution analysis, testes and other relevant organs were collected, embedded fresh in optimal cutting temperature (O.C.T.) compound, flash-frozen on dry ice, and stored at −80 °C until sectioning. Cryostat sections (5 µm) were mounted on glass slides, briefly fixed in 4% paraformaldehyde (PFA) or acetone, counterstained with DAPI, and mounted in antifade medium.

Immunofluorescence staining of testis sections:
Other testis samples were fixed in 4% PFA (overnight at 4 °C), dehydrated, cryoprotected in 30% sucrose, and sectioned at 5 µm. After washing in PBS, sections underwent heat-mediated antigen retrieval (10 min in citrate buffer pH 6.0). Blocking was performed in 5% normal goat serum with 0.1% Triton X-100 for 1 h. Primary antibodies were incubated overnight at 4 °C: SOX9 (HuaBio, Cat# ET1611-56, 1:500), PRM1 (Briar Patch, Hup-1N, 1:200), and HA-tag (CST, clone C29F4, 1:500). Alexa Fluor 488–conjugated peanut agglutinin (PNA, Thermo Fisher L21409; 2 µg/mL) was used for acrosomes. After PBS washes, slides were incubated for 1 h with Alexa Fluor 488 goat anti-rabbit (Invitrogen A-11008, 1:500) and Alexa Fluor 594 goat anti-mouse (Invitrogen A-11005, 1:500). Nuclei were counterstained with DAPI. Imaging was performed on a Zeiss Axio Imager.M2 microscope with fixed acquisition settings across groups.

Histological analysis

For general assessment of morphology and toxicity, testes were fixed in Bouin's solution overnight at 4 °C, transferred to 70% ethanol, dehydrated, and paraffin embedded. Sections (3 µm) were stained with hematoxylin and eosin (H&E) using standard protocols. Slides were examined by a blinded observer. Features evaluated included seminiferous tubule structure, presence or absence of elongating/elongated spermatids, epithelial height, and interstitial integrity. Pathological signs such as germ cell degeneration, vacuolization, multinucleated cells, or disrupted tubule organization were recorded. Images were taken for documentation and compared to age-matched controls.

Intracytoplasmic sperm injection (ICSI) and offspring / fertility analysis

ICSI was performed using testicular sperm from treated males. Mature metaphase II oocytes were obtained from superovulated C57BL/6J females (6–8 weeks) induced with PMSG (NSHF, Cat#110254564) and hCG (NSHF, Cat#A2212051). Cumulus–oocyte complexes were harvested 14 h post-hCG, cumulus cells removed with hyaluronidase (300 µg/mL; Sigma, H4272), and denuded oocytes maintained in KSOM medium (AibeiBio, M1435) under mineral oil (Sigma, M5310-500ML).

Testes from treated males (10–13 days post-injection) were digested with collagenase IV (0.4 mg/mL; Worthington LS004188) and DNase I (10 µg/mL; Roche 10104159001), followed by trypsin-EDTA (0.25%; Gibco 25200072). Digestion was quenched with FBS. Suspensions were filtered, centrifuged, and resuspended in GBSS + 5% FBS + DNase I. Only morphologically normal motile or twitching spermatozoa were selected.

ICSI was performed essentially as described[47,48] using a piezo-electric manipulator (Eppendorf PiezoXpert). Individual sperm were drawn tail-first into injection pipettes (6.5–8.5 µm ID) containing polyvinylpyrrolidone (Vitrolife, 10111). After injection, embryos were cultured to the 2-cell stage (24 h) and transferred into pseudopregnant ICR females (8–10 embryos per oviduct). Litters were delivered naturally. Offspring were monitored for growth, health, endocrine status, fertility, and overall development.

Behavioral assays and sexual activity

Behavioral assays were performed during the light phase after a 1-week habituation.

Open field test[49]: Mice were placed in a 40 × 40 × 40 cm Plexiglass arena for 10 min under 650 lux illumination. Activity was video recorded and analyzed using EthoVision XT. Measures: distance traveled, average speed, and time spent in center vs. periphery. Arenas were cleaned with 70% ethanol between trials.

Novel object recognition test[50]: Day 1: habituation. Day 2: exposure to two identical objects for 10 min. Day 3: one object replaced with a novel one. Recognition index = time with novel / (time novel + time familiar) × 100%.

Object location memory test: Same as NOR, except one object was moved to a new position on Day 3. Location index = time with moved / (time moved + time stationary).

Sexual activity assay[51]: Female mice (≥6 weeks old) were bilaterally ovariectomized under isoflurane anesthesia, given postoperative antibiotics and analgesics, and housed singly until recovery. To induce estrus, females received estradiol benzoate (20 µg in 0.1 mL olive oil, i.p.) 48 h before testing and progesterone (500 µg in 0.1 mL oil, i.p.) 4 h before testing. Estrous status was confirmed by vaginal smears. Sexual behavior tests were conducted in a 40 × 40 × 40 cm Plexiglass open-field arena under dim light at the beginning of the dark cycle. Males were habituated to the apparatus for 2 days. Interactions with primed females were video-recorded for 30 min. Metrics: mounting latency, intromission latency, ejaculation latency, post-ejaculatory interval, copulatory series number and duration, number of mounts and intromissions. Apparatus was cleaned with 75% ethanol after each test. Observers were blinded to groups.

Gene expression (qRT-PCR) & Protein analysis

qRT-PCR: RNA was extracted from flash-frozen testes or other tissues with TRIzol (Thermo Fisher 10296028), DNase treated (Turbo DNase, Thermo AM2239), quantified, and reverse transcribed with HiScript III RT SuperMix (Vazyme R323-01). qPCR was performed on a BIO-RAD CFX-96 with SYBR Green master mix (Vazyme Q712-02). Primers spanned exon–exon junctions (see Supplementary Table 2). *Actb* served as housekeeping control. Reactions were run in triplicate. Relative expression was calculated using the ΔΔCq method with efficiency correction[52]. Specificity was validated by melt curves and gel electrophoresis.

Western blot: Proteins were extracted in NP40 buffer (Sangon Biotech 9016-45-9) with protease inhibitors, quantified by BCA assay, separated by SDS–PAGE, transferred to PVDF membranes (PALL BSP0161), and probed with anti-HA (CST C29F4, 1:1000) and anti-GAPDH (Proteintech 60004-1-Ig, 1:5000). HRP-conjugated secondaries and ECL detection (Thermo 34577) were used. Each experiment included 3 biological replicates.

Hematology and serum biochemistry

Blood was collected via retro-orbital sinus or cardiac puncture. CBCs were measured with Sysmex xn9000. Serum biochemistry (ALT, AST, ALP, bilirubin, BUN, creatinine, electrolytes, glucose) was measured using HITACHI LABOSPECT 008 AS. Analyses were performed blinded to group identity.

Imaging of LNPs by Transmission Electron Microscopy (TEM)

For TEM observation, 5 μL of each LNP sample was applied to a carbon-coated copper grid and allowed to adsorb for ~1 min at room temperature. Excess liquid was then removed with filter paper, followed by negative staining with 2% uranyl acetate for 45–60 s. The grid was blotted dry and air-dried before imaging. TEM images were acquired using a Tecnai G2 Spirit BioTwin transmission electron microscope (FEI, USA) operated at 120 kV. Additionally, for fluorescence microscopy assessment, 5 μL of LNP

dispersion (with fluorescent tracer incorporated) was spotted on a glass slide, air-dried in the dark for ~30 min, and then imaged by epifluorescence microscopy to qualitatively examine LNP fluorescence signals.

Culture and Treatment of Human Seminiferous Tubules

Human seminiferous tubule fragments were obtained from donor testicular tissue under an approved human ethics protocol (No. 20130009). For organ culture, an agarose gel base was prepared by dissolving 0.05 g of agarose in 5 mL ultrapure water, melting it via microwave, and dispensing the solution into a white 96-well plate; the agarose was allowed to cool and solidify at room temperature, forming a half-volume gel layer at the bottom of each well. This soft agarose layer served as a support to maintain an air–medium interface for the explanted tissue[53–55]. Each well was then overlaid with 100 µL of complete culture medium (Procell, CM-H191). Small fragments of human seminiferous tubules were placed in the medium (on top of the gel) and incubated at 33 °C in a humidified 5% CO_2 atmosphere for 1–2 h to equilibrate. Subsequently, Luci MC3 LNP (containing the codon-optimized luciferase mRNA) was added to the wells (typically in a 1:100–1:500 dilution of the stock into the culture medium), and the samples were further incubated under the same conditions for either 24 h or 48 h. After the incubation period (at the designated 24 h or 48 h endpoint), the medium was removed from each well. Then, 100 µL of a detection working solution – composed of 50 µL culture medium mixed with 50 µL of luciferase substrate reagent (Beyotime, Cat. RG043M) – was added to each well, directly covering the tubule fragments. After a 5 min incubation at room temperature to allow substrate penetration and signal development, bioluminescence from the luciferase-expressing tubule fragments was measured using a Spark multimode microplate reader (Tecan), with an integration time of 0.5 s per well. (Luminescence readings were performed for both 24 h and 48 h treated samples to assess transfection efficacy over time.)

Fluorescence "Squash" Immunostaining

To visualize luciferase expression within the seminiferous tubule cells, a squash immunostaining technique was employed. Cultured human tubule fragments were first fixed in 2% paraformaldehyde (in 1× PBS containing 0.1% Triton X-100) for 5–10 min at room temperature. Each fragment was then gently placed on a glass microscope slide, overlaid with a coverslip, and lightly pressed to flatten the tubule ("squash" preparation). The slide with coverslip was quickly plunged into liquid nitrogen, freezing the sample. Once frozen, the coverslip was pried off, leaving the flattened tubule tissue adhered to the slide. The slides were stored at −80 °C until immunostaining. For staining, slides were brought to room temperature and washed three times with PBS (5 min each). The tissue was then incubated overnight at 4 °C in a humidified chamber with primary antibody against firefly luciferase (rabbit polyclonal, Abcam ab185924, 1:500 dilution in PBS). The next day, slides were washed in PBS three times (10 min each). A secondary antibody (goat anti-rabbit IgG conjugated to Alexa Fluor 488, Invitrogen A11008) diluted 1:500 in PBS was applied to the samples, and slides were incubated for 1–2 h at room temperature in the dark. After secondary incubation, slides were washed again in PBS (3 × 10 min). Finally, samples were mounted with Vectashield antifade medium containing DAPI (Vector Laboratories H-1200) to counterstain nuclei, and a coverslip was applied and sealed with nail polish. Immunofluorescence images were captured using a fluorescence microscope. The resulting images allowed identification of Luci mRNA-translated protein (luciferase) within the tubule cells (green fluorescence), alongside nuclear staining (blue).

TUNEL Assay for Apoptosis Detection in Testis

Apoptotic cells in mouse testes were detected using a one-step TUNEL (TdT-mediated dUTP nick-end labeling) in situ apoptosis detection kit (Elabscience, Cat. E-CK-A321, FITC Green). Whole testes from mice were fixed in 4% paraformaldehyde (pH 7.4) at 4 °C overnight, then cryoprotected by soaking in 30% sucrose, embedded in OCT compound, and cryosectioned at 5 μm thickness. Frozen sections were equilibrated to

room temperature, then post-fixed in 4% PFA for 30 min and washed with PBS (3 × 5 min). Sections were permeabilized with 100 μL of Proteinase K working solution at 37 °C for 20 min, followed by three PBS washes. Next, 100 μL of TdT Equilibration Buffer was applied for 20 min at 37 °C, and subsequently 50 μL of TUNEL reaction mixture (label and enzyme) was added to each section. Slides were incubated in a humidified chamber at 37 °C for 1 h in the dark. For negative-control sections, the TdT enzyme was omitted (to confirm specificity of staining), while for positive controls, sections were pre-treated with DNase I to fragment DNA before TUNEL labeling. After the 1 h incubation, sections were washed with PBS (3 × 5 min), then counterstained with DAPI for 5 min to label nuclei. After four final rinses in PBS, sections were mounted with antifade medium and coverslipped. Fluorescent images of the sections were acquired (TUNEL-positive nuclei appearing as green punctate nuclear fluorescence). Using ImageJ software, the apoptotic index in each section was quantified as described[56]. TUNEL fluorescence intensity (gray value) was measured to indicate the apoptotic signal, while DAPI-stained nuclear area was used to normalize for total cell number. The apoptotic index was calculated as the ratio of TUNEL gray value to total DAPI-positive nuclear area, representing the mean optical density of the TUNEL signal per seminiferous tubule.

Hormone Measurement by ELISA

Testicular hormone levels were measured by enzyme-linked immunosorbent assay (ELISA). In particular, testosterone and follicle-stimulating hormone (FSH) concentrations in culture media (or serum, as applicable) were quantified using commercial ELISA kits: Testosterone ELISA Kit (SIMI BIO, Cat. ME-M1435S) and FSH ELISA Kit (SIMI BIO, Cat. ME-M1539S). All procedures were carried out according to the manufacturers' instructions. At the conclusion of the culture or treatment period, samples were collected and incubated with the kit's assay reagents in 96-well plate format. Absorbance readings were taken on a microplate spectrophotometer, and

hormone concentrations were calculated based on the standard curves provided in the kit manuals. Results were reported in ng/mL for testosterone and mIU/mL for FSH, consistent with kit specifications.

Primers and antibodies

Primer sequences (e.g., *Papolb* forward 5′-CTGTCCATCGACCTGACTTATG-3′; reverse 5′-GCAACTGGTGCAGTTCTTTC-3′; *Actb* forward 5′-TCTAGACTTCGAGCAGGAGATG-3′; reverse 5′-GAACCGCTCGTTGCCAATA-3′) are listed in Supplementary Table 2. Antibody information (host, catalog number, lot, dilution) is also in Supplementary Table 2. Specificity was validated by omission and isotype controls.

Statistical analysis

All data are shown as mean ± s.d. unless stated otherwise. GraphPad Prism v9 was used. Two-group comparisons: unpaired two-tailed Student's t-test (if normality passed) or Mann–Whitney U test (if not). Multi-group comparisons: one-way or two-way ANOVA with Tukey's or Bonferroni post hoc correction. Threshold for significance: $P < 0.05$. Significance reported as $P < 0.05$ (**),P<0.01(**),P<0.001(***)*, and *P<0.0001 (****)*. Exact P values provided where possible. Outliers were tested with Grubbs' test ($\alpha = 0.05$). Randomization and blinding were applied where possible. Sample sizes were determined by power analysis and precedent. No animals were excluded except for technical failures, which did not occur in this study.

Acknowledgments

We thank Yuchao Sun, Ying Liu, Lejun Zhang, Yuting Wang, Wenying Long, Yao Wu, and Yunpan Wang from the Core Facilities of the Fourth Affiliated Hospital, Zhejiang University School of Medicine, and of the International Institutes of Medicine, Zhejiang University, for their technical support. We are grateful to Beijia Wang, Laijie Ni,

Xiangfei Zhang, Yulan Zheng, and Weiwei Jin from the Laboratory Animal Center of the International Institutes of Medicine, Zhejiang University, for their meticulous care of the laboratory mice. We also thank the Pathology Core and the Department of Laboratory Medicine of the Fourth Affiliated Hospital, Zhejiang University School of Medicine, as well as members of the Li laboratory, for assistance and helpful discussions. We thank Chenyu Yang in the Center of Cryo-Electron Microscopy (CCEM), Zhejiang University for her technical assistance on Transmission Electron Microscopy. We acknowledge Levostar and GemPharmatech for their contributions to plasmid construction.

Author Contributions

Q.K.J. and Kexin Su prepared the lipid nanoparticle formulations; Q.K.J., Yukai Zhong, and Xuliang Ma performed the in vivo mouse experiments; Huali Luo, Q.K.J., Linlin Zhang, and Haifeng Zhang carried out H&E staining; Jiaoyan Ma performed the TUNEL staining; Q.K.J., Hao Wang, Qiaodan Li, Yukai Zhong, Jingwen Luo, and Xuliang Ma conducted intracytoplasmic sperm injection and embryo transfer; Q.K.J. and Zhihui Zhang performed the complete blood count and serum biochemistry analyses; Jingwen Luo, Q.K.J., and Xuliang Ma conducted the behavioral tests; Q.K.J. and Banghua He carried out Western blot assays; Q.K.J., Yukai Zhong, and Qin Li were responsible for photographing and genotyping the "Papi" and other offspring; X.Z.L. and Q.K.J. analyzed the data; X.Z.L., Xianguang Yang, Lejun Li, Shuai Liu, and Zhefan Yuan contributed to the study design. All authors participated in the preparation of the manuscript.

Competing Interests The authors declare no competing interests.

Author Information The authors declare no competing financial interests. Correspondence and requests for materials should be addressed to xinlirna@zju.edu.cn

Reference

1. Chandra, A., Copen, C. E. & Stephen, E. H. Infertility and impaired fecundity in the United States, 1982-2010: data from the National Survey of Family Growth. *Natl Health Stat Report* 1-18, 1 p following 19 (2013).
2. Logan, S., Gu, R., Li, W., Xiao, S. & Anazodo, A. Infertility in China: Culture, society and a need for fertility counselling. *Asian Pacific Journal of Reproduction* **8**, 1-6 (2019).
3. Plaseska-Karanfilska, D. et al. Genetic causes of male infertility. *Balkan J Med Genet* **15**, 31-34 (2012).
4. Jan, S. Z. et al. Unraveling transcriptome dynamics in human spermatogenesis. *Development* **144**, 3659-3673 (2017).
5. Kothandaraman, N., Agarwal, A., Abu-Elmagd, M. & Al-Qahtani, M. H. Pathogenic landscape of idiopathic male infertility: new insight towards its regulatory networks. *NPJ Genom Med* **1**, 16023 (2016).
6. Hu, L. et al. Assisted reproductive technology in China: results generated from data reporting system by CSRM from 2013 to 2016. *Frontiers in Endocrinology* **11**, 458 (2020).
7. Smith, A. D. A. C., Tilling, K., Nelson, S. M. & Lawlor, D. A. Live-Birth Rate Associated With Repeat In Vitro Fertilization Treatment Cycles. *JAMA* **314**, 2654-2662 (2015).
8. Heller, C. G. & Clermont, Y. Spermatogenesis in man: an estimate of its duration. *Science* **140**, 184-186 (1963).
9. Amann, R. P. & Howards, S. S. Daily spermatozoal production and epididymal spermatozoal reserves of the human male. *J Urol* **124**, 211-215 (1980).
10. Townsend, B. A. Human genome editing: how to prevent rogue actors. *BMC Med Ethics* **21**, 95 (2020).
11. Fijak, M., Bhushan, S. & Meinhardt, A. Immunoprivileged sites: the testis. *Methods Mol Biol* **677**, 459-470 (2011).
12. Luaces, J. P., Toro-Urrego, N., Otero-Losada, M. & Capani, F. What do we know about blood-testis barrier? current understanding of its structure and physiology. *Front Cell Dev Biol* **11**, 1114769 (2023).
13. Iguchi, N., Tobias, J. W. & Hecht, N. B. Expression profiling reveals meiotic male germ cell mRNAs that are translationally up- and down-regulated. *Proc Natl Acad Sci U S A* **103**, 7712-7717 (2006).
14. Sun, Y. H. et al. Single-molecule long-read sequencing reveals a conserved intact long RNA profile in sperm. *Nat Commun* **12**, 1361 (2021).
15. Gapp, K. et al. Alterations in sperm long RNA contribute to the epigenetic inheritance of the effects of postnatal trauma. *Mol Psychiatry* (2018).
16. Domazet-Lošo, T. mRNA vaccines: Why is the biology of retroposition ignored. *Genes* **13**, 719 (2022).
17. Du, S. et al. Cholesterol-Amino-Phosphate (CAP) Derived Lipid Nanoparticles for Delivery of Self-Amplifying RNA and Restoration of Spermatogenesis in Infertile Mice. *Adv Sci (Weinh)* **10**, e2300188 (2023).

18. Mashiko, D. et al. Sperm and offspring production in a nonobstructive azoospermia mouse model via testicular mRNA delivery using lipid nanoparticles. *Proc Natl Acad Sci U S A* **122**, e2516573122 (2025).
19. Jarzebska, N. T., Mellett, M., Frei, J., Kündig, T. M. & Pascolo, S. Protamine-Based Strategies for RNA Transfection. *Pharmaceutics* **13**, (2021).
20. Yamazaki, Y. et al. In vivo gene transfer to mouse spermatogenic cells by deoxyribonucleic acid injection into seminiferous tubules and subsequent electroporation. *Biol Reprod* **59**, 1439-1444 (1998).
21. Michaelis, M., Sobczak, A. & Weitzel, J. M. In vivo microinjection and electroporation of mouse testis. *J Vis Exp* (2014).
22. Buckley, M. et al. Visualizing lipid nanoparticle trafficking for mRNA vaccine delivery in non-human primates. *Mol Ther* **33**, 1105-1117 (2025).
23. Adams, M. D. et al. The genome sequence of Drosophila melanogaster. *Science* **287**, 2185-2195 (2000).
24. Monroe, J. et al. N1-Methylpseudouridine and pseudouridine modifications modulate mRNA decoding during translation. *Nat Commun* **15**, 8119 (2024).
25. Hedger, M. P. Toll-like receptors and signalling in spermatogenesis and testicular responses to inflammation--a perspective. *J Reprod Immunol* **88**, 130-141 (2011).
26. Li, N., Wang, T. & Han, D. Structural, cellular and molecular aspects of immune privilege in the testis. *Front Immunol* **3**, 152 (2012).
27. Kashiwabara, S. et al. Regulation of spermatogenesis by testis-specific, cytoplasmic poly(A) polymerase TPAP. *Science* **298**, 1999-2002 (2002).
28. Kashiwabara, S. I., Tsuruta, S., Okada, K., Yamaoka, Y. & Baba, T. Adenylation by testis-specific cytoplasmic poly(A) polymerase, PAPOLB/TPAP, is essential for spermatogenesis. *J Reprod Dev* **62**, 607-614 (2016).
29. Clermont, Y. & Trott, M. Duration of the cycle of the seminiferous epithelium in the mouse and hamster determined by means of 3H-thymidine and radioautography. *Fertil Steril* **20**, 805-817 (1969).
30. Baudat, F., Manova, K., Yuen, J. P., Jasin, M. & Keeney, S. Chromosome synapsis defects and sexually dimorphic meiotic progression in mice lacking Spo11. *Mol Cell* **6**, 989-998 (2000).
31. Romanienko, P. J. & Camerini-Otero, R. D. The mouse Spo11 gene is required for meiotic chromosome synapsis. *Mol Cell* **6**, 975-987 (2000).
32. Zhou, L. et al. BTBD18 Regulates a Subset of piRNA-Generating Loci through Transcription Elongation in Mice. *Dev Cell* **40**, 453-466.e5 (2017).
33. Maier, M. A. et al. Biodegradable lipids enabling rapidly eliminated lipid nanoparticles for systemic delivery of RNAi therapeutics. *Mol Ther* **21**, 1570-1578 (2013).
34. Hassett, K. J. et al. Optimization of Lipid Nanoparticles for Intramuscular Administration of mRNA Vaccines. *Mol Ther Nucleic Acids* **15**, 1-11 (2019).
35. Ren, Y. et al. Impact of ionizable lipid type on the pharmacokinetics and biodistribution of mRNA-lipid nanoparticles after intravenous and subcutaneous injection. *J Control Release* **384**, 113945 (2025).

36. Ferraresso, F. et al. Comparison of DLin-MC3-DMA and ALC-0315 for siRNA Delivery to Hepatocytes and Hepatic Stellate Cells. *Mol Pharm* **19**, 2175-2182 (2022).
37. Escalona-Rayo, O. et al. In vitro and in vivo evaluation of clinically-approved ionizable cationic lipids shows divergent results between mRNA transfection and vaccine efficacy. *Biomed Pharmacother* **165**, 115065 (2023).
38. Carrasco, M. J. et al. Ionization and structural properties of mRNA lipid nanoparticles influence expression in intramuscular and intravascular administration. *Commun Biol* **4**, 956 (2021).
39. Couture-Senécal, J., Natraj, J. & Khan, O. F. A Cell-Free Kinetic Analysis of Ionizable Lipid Hydrolysis. *Anal Chem* **96**, 17128-17134 (2024).
40. Ferraresso, F. et al. Comparison of DLin-MC3-DMA and ALC-0315 for siRNA Delivery to Hepatocytes and Hepatic Stellate Cells. *Mol Pharm* **19**, 2175-2182 (2022).
41. Van Voorhis, B. J. et al. Effect of the total motile sperm count on the efficacy and cost-effectiveness of intrauterine insemination and in vitro fertilization. *Fertil Steril* **75**, 661-668 (2001).
42. Le Goff, A., Jeffries Hein, R., Hart, A. N., Roberson, I. & Landecker, H. L. Anticipating in vitro gametogenesis: Hopes and concerns for IVG among diverse stakeholders. *Stem Cell Reports* **19**, 933-945 (2024).
43. Noguchi, Y., Maruoka, M. & Suzuki, J. Protocol for in vivo CRISPR screening targeting murine testicular cells. *STAR Protoc* **5**, 103306 (2024).
44. Claustres, M. Molecular pathology of the CFTR locus in male infertility. *Reprod Biomed Online* **10**, 14-41 (2005).
45. Su, K. et al. Reformulating lipid nanoparticles for organ-targeted mRNA accumulation and translation. *Nat Commun* **15**, 5659 (2024).
46. Mizuno-Iijima, S. et al. Mouse resources at the RIKEN BioResource Research Center and the National BioResource Project core facility in Japan. *Mamm Genome* **33**, 181-191 (2022).
47. Yoshida, N. & Perry, A. C. Piezo-actuated mouse intracytoplasmic sperm injection (ICSI). *Nat Protoc* **2**, 296-304 (2007).
48. Tang, J. et al. Monitoring Blood Glucose in Mouse Offspring after Intracytoplasmic sperm injection - Embryo Transfer. *J Vis Exp* (2024).
49. Gould, T. D. *Mood and Anxiety Related Phenotypes in Mice* (Humana Press, 2016).
50. Leger, M. et al. Object recognition test in mice. *Nat Protoc* **8**, 2531-2537 (2013).
51. Liu, Z. W. et al. Assessment of Sexual Behavior of Male Mice. *J Vis Exp* (2020).
52. Peirson, S. N., Butler, J. N. & Foster, R. G. Experimental validation of novel and conventional approaches to quantitative real-time PCR data analysis. *Nucleic Acids Res* **31**, e73 (2003).
53. Gholami, K., Pourmand, G., Koruji, M., Ashouri, S. & Abbasi, M. Organ culture of seminiferous tubules using a modified soft agar culture system. *Stem Cell Res Ther* **9**, 249 (2018).

54. Song, K. et al. Targeting APLN/APJ restores blood-testis barrier and improves spermatogenesis in murine and human diabetic models. *Nat Commun* **13**, 7335 (2022).
55. Li, C. et al. Lovastatin promotes the self-renewal of murine and primate spermatogonial stem cells. *Stem Cell Reports* **18**, 969-984 (2023).
56. de Noiron, J., Hoareau, M., Colin, J. & Guénal, I. Apoptosis Quantification in Tissue: Development of a Semi-Automatic Protocol and Assessment of Critical Steps of Image Processing. *Biomolecules* **11**, (2021).

Jiang et al, Fig. 1

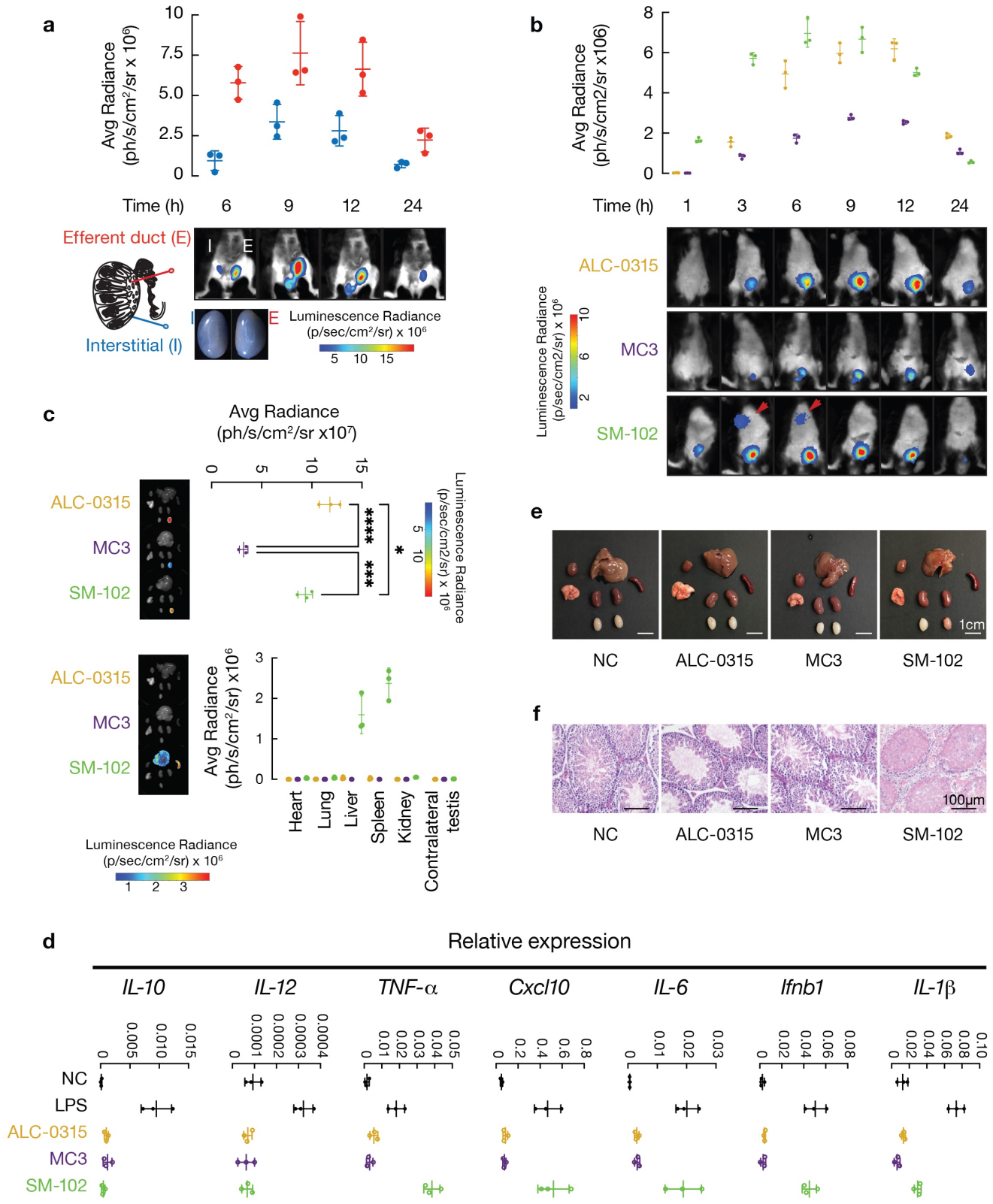

Figure Legends

Figure 1. Efficient intratubular delivery of mRNA via LNPs and biodistribution assessment. (a) Bioluminescence imaging comparing luciferase expression in the testis following two injection routes in the same mouse. The "E" testis received an efferent duct (rete testis) infusion of luciferase mRNA LNP, and the "I" testis received a direct interstitial injection. (b) In vivo bioluminescence images of a representative mouse over 1–24 h after intratubular injection of luciferase mRNA LNP (images show the 1 h and 24 h time points for each formulation). (c) Ex vivo luciferase activity 12 h post-injection in major organs (photons s^{-1} cm^{-2} sr^{-1}, logarithmic scale). Data are mean ± s.d. (n = 3 mice per group). (d) Innate immune response in the testis after mRNA LNP delivery. mRNA levels of inflammation-related cytokines in the testis 12 h after luciferase mRNA delivery via different LNP formulations: *Il-10*, *Il-12*, *Tnf-α*, *Cxcl10*, *Il-6*, *Ifnb1* and *Il-1β*. Black bars indicate untreated control testes; purple bars are MC3 LNP–treated; gold bars are ALC-0315 LNP–treated; green bars are SM-102 LNP–treated; and black bars are a positive control (intraperitoneal LPS injection). Data are mean ± s.d. (n = 3 mice per group). (e) Gross appearance of a testis 12 h after LNP injection. The SM-102 injected testis (rightmost panel) is visibly enlarged, red and inflamed compared to a control testis (leftmost panel). Testes injected with MC3 or ALC-0315 LNPs show no such gross changes. Other organs (liver, spleen, kidney, etc.) appear similar across groups. Scale bar: 1 cm. (f) H&E-stained sections of testes 12 h after injection of 10 μg luciferase mRNA LNPs. The SM-102–injected testis (right) shows interstitial edema and leukocyte infiltration, indicating acute inflammation. In contrast, testes injected with ALC-0315 (mid-left) or MC3 LNP (mid-right) appear histologically normal with no significant inflammatory infiltrate. Scale bar: 100 μm.

Jiang et al, Fig. 2

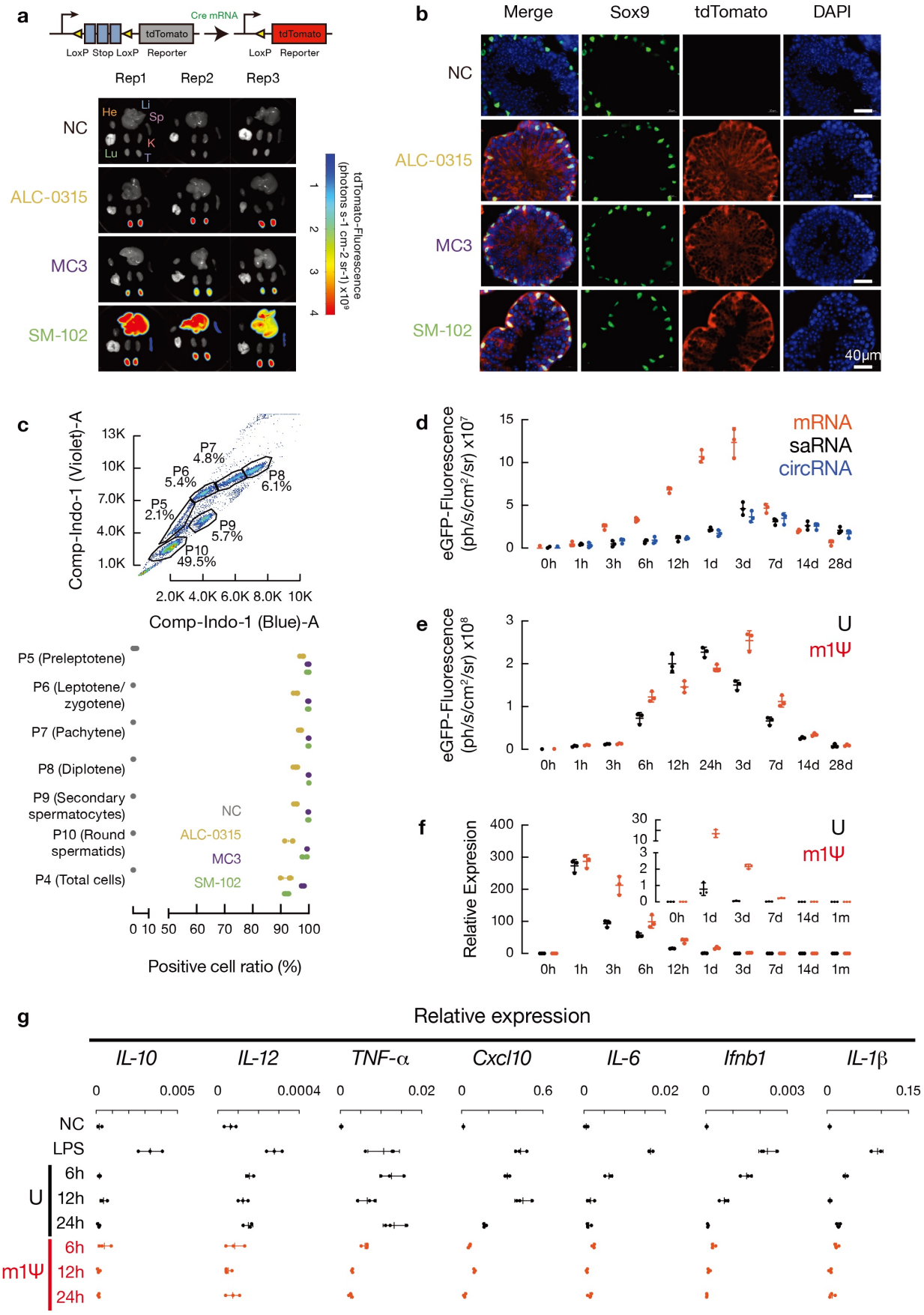

Figure 2. High-efficiency germ cell transfection and benefits of modified mRNA. (a) **Upper:** Schematic of the Ai9 Cre-reporter system. In Ai9 mice, a LoxP-flanked STOP cassette prevents tdTomato expression until Cre recombinase excises the STOP, activating red fluorescence in any cell that has received Cre.
Lower: In vivo fluorescence imaging of Ai9 mice 48 h after intratubular injection of Cre mRNA LNP (n = 3 mice per group). H, heart; Lu, lung; Li, liver; S, spleen; K, kidney; T, testis. (b) A seminiferous tubule cross-section from a treated testis, co-stained for tdTomato (red), the Sertoli cell marker SOX9 (green), and nuclei (DAPI, blue). Scale bar: 40 µm. (c) **Upper:** Gating strategy to resolve stages: pre-leptotene spermatogonia (2N, within P5), leptotene/zygotene spermatocytes (replicating DNA, P6), pachytene spermatocytes (4N, mid-meiosis, P7), diplotene spermatocytes (4N, late meiosis, P8), secondary spermatocytes (2N, post-meiosis II, P9) and round spermatids (1N, P10).
Lower: Percentage of tdTomato-positive cells within each gated population for ALC-0315, MC3 versus SM-102 LNP–Cre-treated testes (48 h post-injection; n = 6 testes each). (d) Kinetics of eGFP expression in testes following delivery of different RNA formats. Mice were injected (via MC3 LNP) with either N^1mΨ-modified eGFP mRNA (red), self-amplifying RNA replicon (saRNA, black) or circular RNA (circRNA, blue) encoding eGFP. Plotted is the radiant efficiency (GFP fluorescence) of the injected testis over 14 days (mean ± s.d.; n = 3 mice per group). (e) Time-course comparison of unmodified versus pseudouridine-modified mRNA (both encoding eGFP). Unmodified mRNA (black) drives an early peak of GFP (within 1 day) followed by a steep decline; modified mRNA (red) shows a delayed peak (~3 days) and a slower decline (mean ± s.d.; n = 3 mice per group). (f) RT-qPCR measurement of eGFP mRNA in the testis at various times after injection of unmodified versus modified eGFP mRNA. (g) Innate immune gene induction in the testis by unmodified versus modified mRNA. RT-qPCR measurements were taken at 6, 12 and 24 h after injection of 10 µg eGFP mRNA (either unmodified or N^1mΨ-modified). Data are mean ± s.d. (n = 3 mice per group).

Jiang et al, Fig. 3

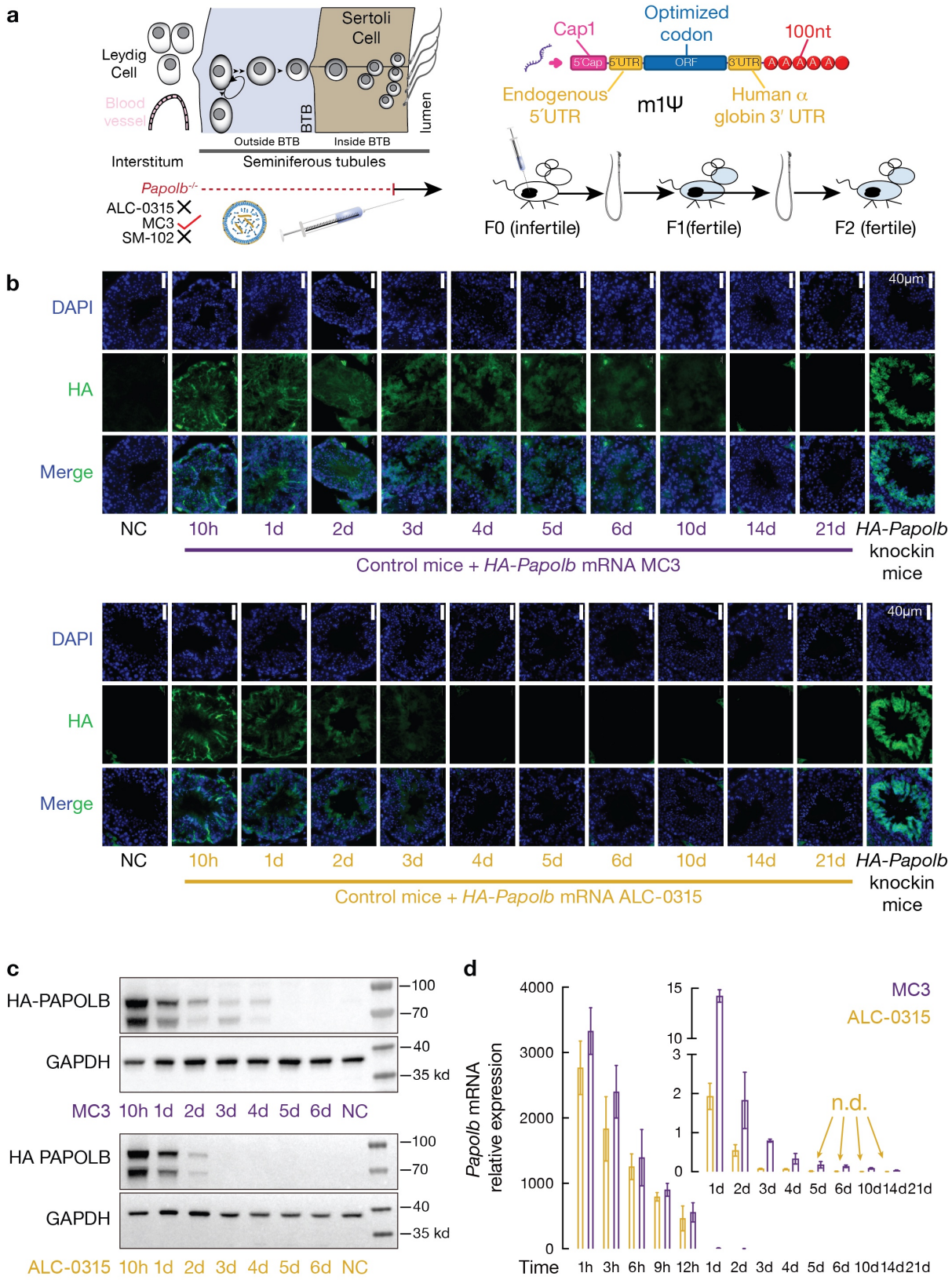

Figure 3. Optimized *Papolb* mRNA formulation sustains expression in testis via MC3 LNP. (a) Graphical abstract of this study with schematic design of *Papolb* mRNA used for therapy. Codon-optimized open reading frame (ORF) plus native 5′UTR and heterologous stabilizing human α-globin 3′UTR; small HA tag for detection. BTB stands for blood-testis barriers. (b) Immunofluorescence detection of HA-tagged PAPOLB protein (green) in a wild-type testis 10 h after injection of MC3 LNP– *Papolb* mRNA. Scale bar: 40 μm. (c) Western blot verification of *Papolb* mRNA expression. Testes from wild-type mice were harvested at the indicated time points after injection with 10 μg HA– *Papolb* mRNA (formulated in MC3 LNP, upper; ALC-0315 LNP, bottom). An anti-HA tag antibody detects a clear band of the expected size (~90 kDa) in lysates from injected testes, whereas no band is present in the uninjected contralateral testis (NC). A GAPDH blot is shown as a loading control. (d) Time-course of *Papolb* mRNA persistence in the testis after delivery by ALC-0315 versus MC3 LNP. RT-qPCR was used to detect *Papolb* mRNA in testes at various times post-injection (mean ± s.d.; n = 3 mice per group per time point).

Jiang et al, Fig. 4

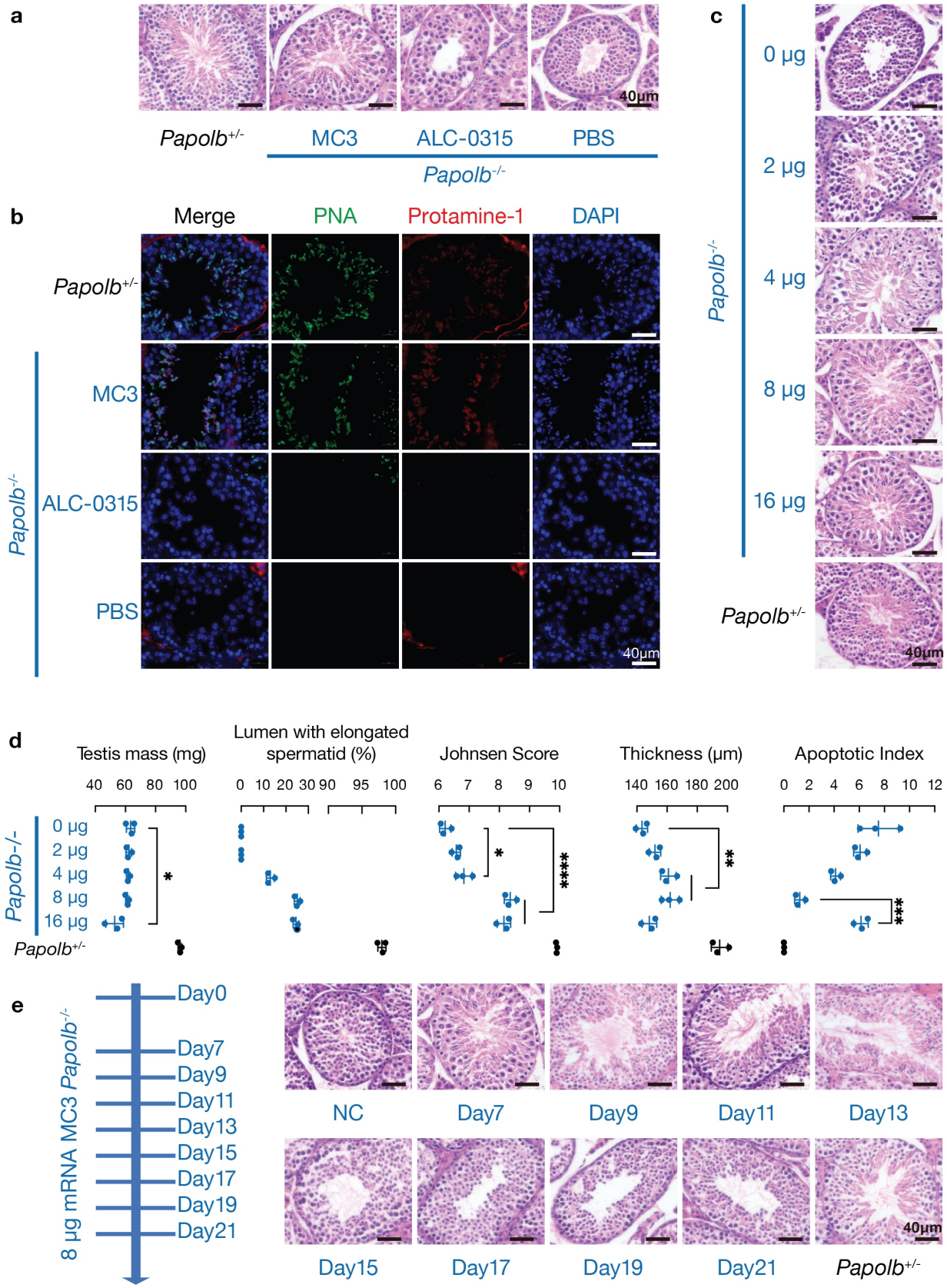

Figure 4. Restoration and transient timeline of spermatogenesis after MC3 LNP–mRNA therapy. (a) H&E-stained cross-sections of seminiferous tubules from *Papolb* mutant and *Papolb*$^{+/-}$ (heterozygous control) mice (7 days post-treatment). Scale bar: 40 µm. (b) Immunofluorescence for protamine-1 (red) on testis sections from *Papolb*-deficient mice 7 days after treatment, and acrosomes are co-stained with PNA lectin (green) and nuclei with DAPI (blue). Scale bar: 40 µm. (c) Testis histology (H&E) for each dose group compared to an untreated *Papolb*$^{+/-}$ heterozygous control. Scale bar: 40 µm. (d) From left to right, five quantifications across dose groups comparing MC3-*Papolb* mRNA LNP treatment in *Papolb* knockout mice, and heterozygous (Het) controls: **Leftmost panel:** Testis mass (average) per group. **Second panel:** Percentage of seminiferous tubules containing elongated spermatids (histological scoring). **Middle panel:** Johnsen score indicating spermatogenic completeness (mean ± s.d.; $n = 3$). **Fourth panel:** Seminiferous tubule epithelial height (germ cell layer thickness) measured in H&E sections. **Rightmost panel:** Apoptotic index quantified by TUNEL staining, calculated as the ratio of TUNEL gray value to total DAPI-positive nuclear area, representing the mean optical density of TUNEL signal per seminiferous tubule. (e) (left) Scheme of the timing after treatment. (right) H&E-stained testis sections from *Papolb*-deficient mice at various time points after a single 8 µg MC3– *Papolb* mRNA injection. Scale bar: 40 µm.

Jiang et al, Fig. 5

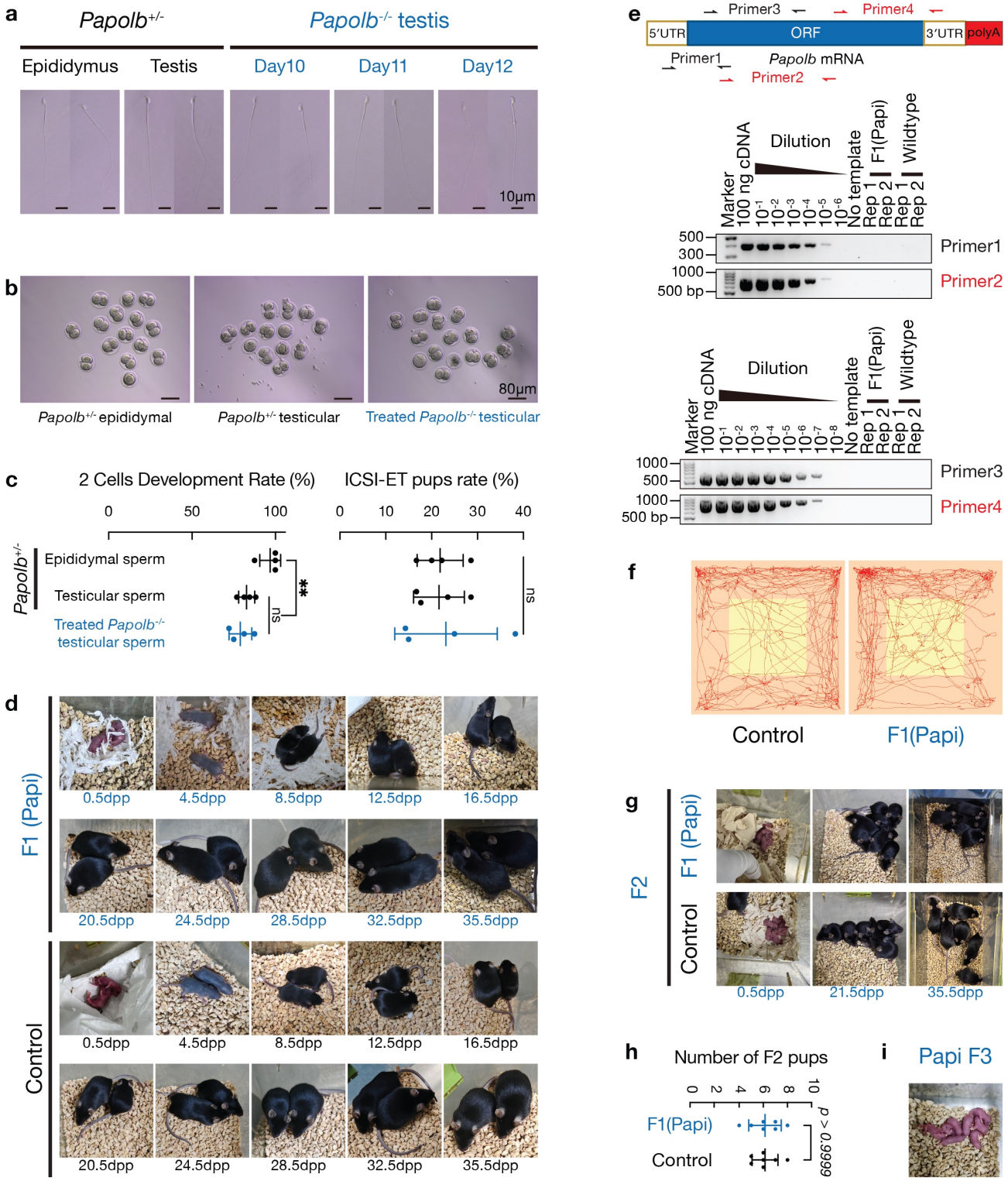

Figure 5. Restored spermatogenesis enables functional fertility. (a) Bright-field images of motile spermatozoa isolated from testes ~10–12 days post-treatment. Left: two epididymis sperm; Middle: two testicular sperm from a *Papolb*$^{+/-}$ heterozygous control male (normal spermatogenesis). Right: a rescued testicular sperm from a *Papolb*-deficient male treated with MC3 LNP–*Papolb* mRNA. The rescued mutant sperm shows normal morphology (oval head with hook and a long tail) comparable to control. Scale bar: 10 µm. (b) Two-cell embryo formation using different sperm sources for ICSI. Scale bar: 80 µm. (c) (left) Two-cell embryo formation rates Bars represent the percentage of injected oocytes that developed into two-cell embryos by 24 h. (right) Percentage of transferred embryos that resulted in live pups (embryo transfer success rate). Error bars show s.d. for four independent experiments.
(d) Healthy offspring obtained by ICSI using rescued *Papolb*-deficient sperm. Images show representative pups from *Papolb*-deficient sires treated with mRNA (upper panel, ages 0.5 to 35.5 days postpartum) alongside age-matched control pups from a *Papolb*$^{+/-}$ father (lower panel). (e) PCR analysis of offspring genomic DNA to check for potential integration of the *Papolb* mRNA transgene. Serial dilutions of cDNA were made to determine the detection limit of four different primer sets targeting distinct regions of *Papolb* mRNA. Bands from these dilutions were sequenced to confirm that amplification was specific to in vitro-transcribed *Papolb* mRNA. (f) Representative locomotor tracks from the open-field test. (g) Growth and morphology of F2 offspring: Representative pups at 0.5 days, 21.5 days, and 35.5 days postpartum from F1 parents. (h) Pup size measurements of F1 offspring derived from rescued *Papolb*-deficient sires versus *Papolb*$^{+/-}$ controls. (i) Morphology of F3 offspring derived from rescued *Papolb*-deficient lineage: Representative pups at ~0.5 days postpartum from F2 parents.

Jiang et al, Fig. 6

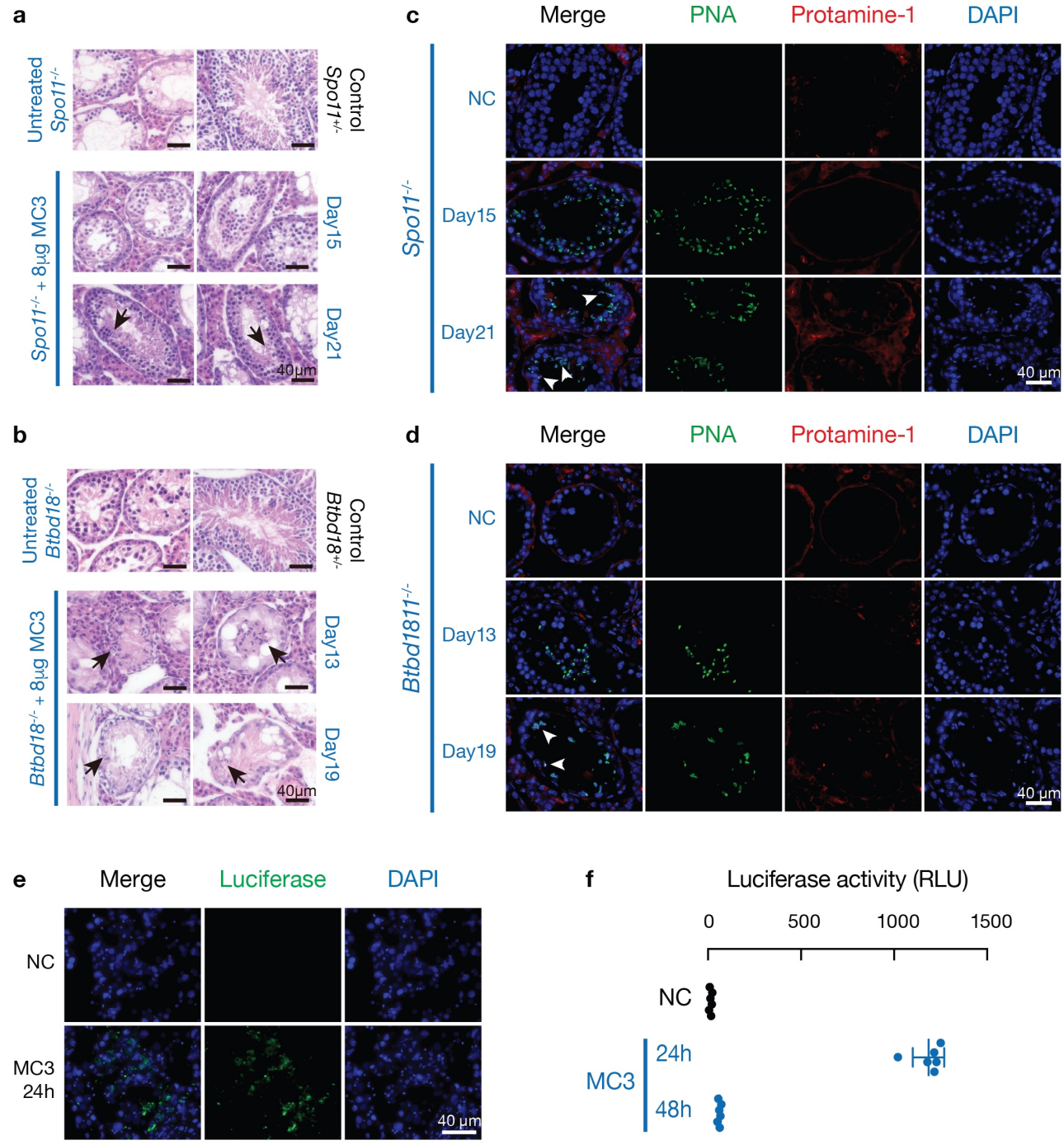

Figure 6. Generalizability of the mRNA–LNP therapeutic platform to diverse genetic male-infertility models and human tissue. (a) *Spo11* knockout mice treated with *Spo11* mRNA–LNP. Elongated spermatids are indicated by arrows. (b) *Btbd18* knockout mice treated with the corresponding *Btbd18* mRNA–LNP. Elongated spermatids are indicated by arrows. (c,d) Immunofluorescence staining of testes from treated models showing co-localization of Protamine-1 (red; late-stage spermiogenesis marker), PNA-lectin (green; acrosome marker) and DAPI (blue; nuclei). (c) *Spo11* knockout testes at days 15 and 21 post-treatment show the appearance of elongating and elongated spermatids (arrowheads). (d) *Btbd18* knockout testes at days 13 and 19 post-treatment display elongating spermatozoa within the seminiferous-tubule lumina (arrowheads). Scale bar, 40 µm. (e) Immunofluorescence of squash preparations from cultured human seminiferous tubules 24 h after exposure to MC3–luciferase mRNA LNPs, revealing luciferase protein (green) in germ cells. DAPI (blue) labels nuclei. Scale bar, 40 µm. (f) Quantification of luminescence (relative light units, RLU) from human seminiferous-tubule cultures at 0, 24, and 48 h following LNP exposure.